Analysis of Model Based Virtual Sensing Techniques for Active Noise Control

Plewe, Daniel; Agerkvist, Finn T.; Fernandez Grande, Efren; Brunskog, Jonas

Published in:
Proceedings of inter-noise 2020

Publication date:
2020

Document Version
Peer reviewed version

Analysis of Model Based Virtual Sensing Techniques for Active Noise Control

Daniel Plewe[1]
Technical University of Denmark
Department of Electrical Engineering
Ørsteds Plads
Building 352
2800 Kgs. Lyngby

Finn T. Agerkvist[2]
Technical University of Denmark
Department of Electrical Engineering
Ørsteds Plads
Building 352
2800 Kgs. Lyngby

Efren Fernandez Grande[3]
Technical University of Denmark
Department of Electrical Engineering
Ørsteds Plads
Building 352
2800 Kgs. Lyngby

Jonas Brunskog[4]
Technical University of Denmark
Department of Electrical Engineering
Ørsteds Plads
Building 352
2800 Kgs. Lyngby

ABSTRACT

The performance of active noise controllers based on adaptive filters like the Filtered Reference Least Mean Square algorithm (FxLMS) is optimal in small zones around the error sensor locations. These locations provide the maximal possible reduction of noise but are not accessible by people due to the presence of the sensors. Virtual sensing algorithms can be applied to move the optimal zone of control away from the error sensors. Such methods have been investigated

[1]daplew@elektro.dtu.dk

[2]fa@elektro.dtu.dk

[3]efg@elektro.dtu.dk

[4]jbr@elektro.dtu.dk

during the last three decades and the most of them rely on initial transfer-function estimation with physical sensors in the virtual locations. This paper investigates how additional physical knowledge about the inherent physics of an active noise control application can be used to derive models, that can extrapolate an arbitrary number of e.g. virtual error sensor signals. A denser grid of error sensors leads to a more homogeneous reduction of noise in a target area and can extend the frequency range of controllability to higher frequencies. The idea of the model based remote microphone technique (MBRMT) is introduced, which is the motivation for this study, and three models for sound-field extrapolation are investigated that could be integrated into the MBRMT.

1. INTRODUCTION

Active noise control based on adaptive filters minimises the error at locations of a set of error sensors. Consequently is the best performance in terms of noise reduction given in places that are not accessible by people. Virtual sensing methods have been developed to overcome this limitation, see [1] for a review of virtual sensing methods. These methods minimise the error in virtual error sensing locations that are remote from the physical sensors. All methods rely on measured or estimated transfer functions, which are then fixed and do not adapt to changing acoustic conditions like a change of air temperature or people entering the virtual error sensing locations. If the conditions change the performance of active control will decrease and the algorithms might diverge. A model that can extrapolate the virtual microphone signals from a set of physical measurements might be able to adapt to changes of the acoustic conditions. Furthermore, the need of measuring transfer functions to the virtual error locations becomes obsolete. This can save massive effort in case many virtual microphones are needed. A dense grid of virtual error sensors can produce a more homogeneous quiet zone area and extend the performance of active control to higher frequencies. The idea of the model based remote microphone technique (MBRMT) will be introduced as the motivation for this paper. The MBRMT makes use of sound field reconstruction in order to predict the sound pressure in remote locations. The focus of this paper will then be on the analysis of three reconstruction methods in order to understand their limitations for the application in active control.

The important parameter of sound-field reconstruction is here the accuracy in predicting the level and phase of a pressure in remote locations. The range in which a minimum accuracy can be guaranteed is of special interest for active control where errors can destabilise the control algorithm. When accurate predictions can be obtained far away from the measurement array, then is the placement of the virtual sensors more flexible. With the virtual sensors moves the actual zone of quiet. While an error in the reconstruction of the pressure level will decrease the insertion loss of active control, so can phase errors of $> |\pm\frac{\pi}{2}|$ cause divergence of the ANC algorithms which needs to be avoided [2].

The reconstruction methods compared here are utilising plane wave decomposition (PWD), the spherical harmonic decomposition (SHD) and the equivalent source method (ESM). These methods are well known and will be quickly reviewed in section 2. All three decompose a set of measurements into a set of basis functions by posing an inverse problem. The obtained coefficients will then be used to predict the sound pressure in remote locations. The inverse problems might be ill-posed, presumably under-determined in the most cases, since there will be most likely fewer measurements available than basis-functions in the models. Solution to these inverse ill-posed problems can be found via e.g., a regularized least squares inversion (LS), or via sparse reconstruction methods, such as compressive sensing (CS). LS and CS are quickly reviewed in section 2.

2. METHODS

2.1. Model Based Remote Microphone Technique - Contribution

This section presents very quickly the idea of the MBRMT. An in depth analysis will be executed in subsequent research. The method is based on the remote microphone technique (RMT), which has been presented the first time by A. Roure in 1999 [3]. The RMT minimises the error in locations remote from a set of physical sensors. To do this it is needed to measure the secondary paths between the virtual sensors and control sources $\mathbf{G}_{vu}$ and between the physical sensors and control sources $\mathbf{G}_{pu}$. Also the primary paths are needed from the virtual and physical sensors to the primary noise sources: $\mathbf{G}_{vn}$ and $\mathbf{G}_{pn}$. The $\mathbf{G}$ matrices contain multi-channel transfer-functions. With these measurements it is possible to construct a matrix $\mathbf{M_1}$ that transforms the estimated primary noise contribution at the physical sensors $\mathbf{d}_p$ to the respective contribution at the virtual sensors $\mathbf{d}_v$. $\mathbf{e}_p$ is the error at the physical sensors, $\mathbf{e}_v$ the error at the virtual sensors, $\mathbf{u}$ the control signal, and $\mathbf{y}_p$ and $\mathbf{y}_v$ the contribution of the secondary sources at the physical and virtual sensors respectively.

$$\mathbf{d}_v = \mathbf{M_1}\mathbf{d}_p, \quad \text{with} \quad \mathbf{M}_1 = \mathbf{G}_{vn}\mathbf{G}_{pn}^{-1} \quad \text{and} \quad \mathbf{d}_p = \mathbf{e}_p - \mathbf{G}_{pu}\mathbf{u}. \tag{1}$$

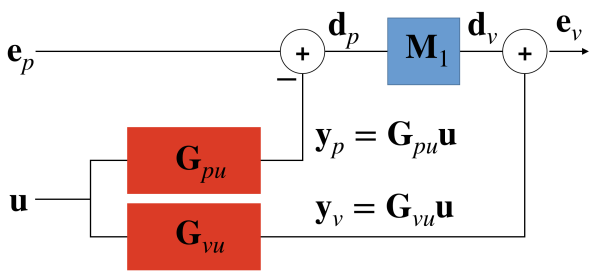

Figure 1: The scheme of the The Remote Microphone Technique

The estimated virtual error $\mathbf{e}_v = \mathbf{d}_v + \mathbf{G}_{vu}\mathbf{u}$ and the virtual secondary path $\mathbf{G}_{vu}$ are then used to update the control filter $\mathbf{w}(\omega, L)$ with the FxLMS update equation 2 at each frequency ω in block L.

$$\mathbf{w}(\omega, L+1) = \mathbf{w}(\omega, L) - \lambda \mathbf{F}_x^H \mathbf{e}_v(\omega, L), \tag{2}$$

with $\mathbf{F}_x = \mathbf{G}_{vu}(\omega)x(\omega, L)$, the filtered reference signal. The filter $\mathbf{w}$ is then used to update the control signal $\mathbf{u} = \mathbf{w}x$. Equation 2 is the most basic block based FxLMS algorithm in frequency domain. Its derivation and numerous derivatives can be studied in [2, 4]. Note that for the measurement of all involved transfer functions it is needed to place physical sensors temporarily at the virtual locations during an initialisation stage. The effort of measuring these transfer-functions can be huge, especially when many physical and virtual error sensors are involved. The access to the primary sources might even be restricted or impossible [5].

The MBRMT replaces the matrix $\mathbf{M}_1$ with a sound field reconstruction method that predicts the contribution of the primary noise in remote locations $\mathbf{d}_v$. The estimate of the virtual error can then be obtained with $\mathbf{e}_v = \mathbf{d}_v + \mathbf{y}_v$. $\mathbf{y}_v$ is not yet available and can be predicted via extrapolation from $\mathbf{y}_p = \mathbf{G}_{vu}\mathbf{u}$. The virtual secondary path can be estimated via the extrapolation matrix $\mathbf{M}_2$ e.g., with $\mathbf{G}_{vu} = \mathbf{M}_2\mathbf{G}_{pu}$. Figure 2 shows the block-diagram of the MBRMT.

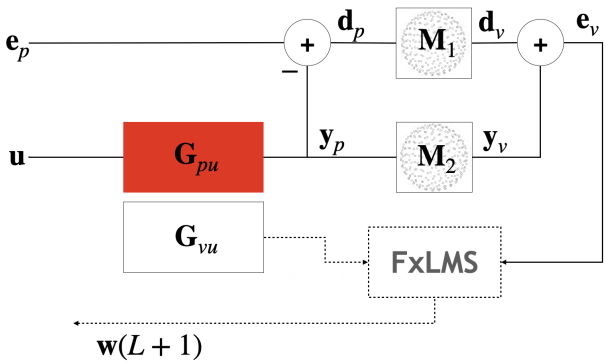

Figure 2: The Model Based Remote Microphone Technique. $\mathbf{M}_1$ *and* $\mathbf{M}_2$ *represent prediction algorithms. The virtual secondary path* $\mathbf{G}_{vu}$ *and the virtual error* $\mathbf{e}_v$ *are used to update the control filter coefficients* $\mathbf{w}(L+1)$ *according to the FxLMS algorithm shown in Equation 2.*

2.2. Extrapolation via plane wave decomposition

A pressure p in location $\mathbf{r}$ in a source free domain Ω can be approximated by a series of plane waves for a constant frequency ω, see also [6].

$$p(\omega, \mathbf{r}) \approx \sum_{j=1}^{N} X_j e^{j\mathbf{k}_j \mathbf{r}} + n(\omega, \mathbf{r}), \tag{3}$$

where X_j is the jth complex coefficient of the jth plane wave and n is additive Gaussian noise. The wave number vector $\mathbf{k}$ indicates the direction of the plane waves and $\mathbf{r}$ is the position vector of the observation point in 3D Cartesian coordinates. This series can be expressed in matrix form.

$$\mathbf{p} = \mathbf{H}\mathbf{x} + \mathbf{n} \tag{4}$$

$\mathbf{H}$ contains the plane-wave basis functions in the rows with direction $\mathbf{k}_j$ and relates them to the observed pressures $\mathbf{p}_i \in \mathbb{C}^M$ in the points $\mathbf{r}_i$ in 3D space with $H_{ij} = e^{j\mathbf{k}_j \mathbf{r}_i}$. The vector $\mathbf{x} \in \mathbb{C}^N$ consists of complex plane wave coefficients and $\mathbf{n}_i = Ae^{j\phi_i}$ is the noise vector with A a constant scalar according to the chosen signal-to-noise-ratio (SNR) and a randomised phase ϕ_i. The solution for $\mathbf{x}$ can be found via the inverse of the matrix with

$$\mathbf{x} = \mathbf{H}^{-1}\mathbf{p}. \tag{5}$$

The inversion of the matrix $\mathbf{H}$ is typically not possible due to the miss-match of the number of basis functions and measurement points. Details about the inversion will be addressed in section 5. With the obtained coefficients vector $\mathbf{x}$ it is possible to predict the pressure $\tilde{\mathbf{p}}$ in arbitrary locations $\mathbf{r}_R \in \Omega$ with

$$\tilde{\mathbf{p}} = \mathbf{H}_R \mathbf{x}. \tag{6}$$

2.3. Extrapolation via spherical harmonics decomposition

The spherical harmonics decomposition or spherical Fourier transform is an established method for sound field analysis [7–9]. When microphones are used to sample the sound-field on the surface of a sphere, centered at the origin, it is possible to describe the measured pressures p_i as a linear combination of spherical harmonics with

$$p_i(r, \theta, \phi) = \sum_{n=0}^{\infty} \sum_{m=-n}^{n} B_{mn} j_n(kr) Y_n^m(\theta, \phi), \tag{7}$$

where $Y_n^m(\theta, \phi)$ are the spherical harmonics describing the angular dependency, j_n is the spherical Bessel function representing the radial dependency and $B_{nm} \in \mathbb{C}$ the coefficients of the transform.

$$Y_n^m(\theta, \phi) = \sqrt{\frac{(2n+1)}{4\pi}\frac{(n-m)!}{(n+m)!}} P_n^m(\cos(\theta)) e^{jm\phi} \tag{8}$$

In order to compute the coefficients B_{nm} Equation 7 can be written in matrix form and the solution expressed via inversion

$$\mathbf{b_j} = \mathbf{Y}^{-1}\mathbf{p}, \tag{9}$$

with the spherical harmonics matrix

$$\mathbf{Y} = \begin{bmatrix} Y_0^0(\theta_1, \phi_1) & Y_1^{-1}(\theta_1, \phi_1) & Y_1^0(\theta_1, \phi_1) & \dots & Y_N^N(\theta_1, \phi_1) \\ Y_0^0(\theta_2, \phi_2) & Y_1^{-1}(\theta_2, \phi_2) & Y_1^0(\theta_2, \phi_2) & \dots & Y_N^N(\theta_2, \phi_2) \\ \dots & \dots & \dots & \dots & \dots \\ Y_0^0(\theta_Q, \phi_Q) & Y_1^{-1}(\theta_Q, \phi_Q) & Y_1^0(\theta_Q, \phi_Q) & \dots & Y_N^N(\theta_Q, \phi_Q) \end{bmatrix} \tag{10}$$

and $b_{j,nm} = B_{mn} j_n(kr)$. Also here will the inversion most likely not be possible and requires the pseudo inverse, e.g. Reconstruction can then be executed as follows

$$\tilde{\mathbf{p}}_R = \mathbf{Y}_R \mathbf{b}, \tag{11}$$

with $\mathbf{b}$ the vector of the coefficients $B_{mn} = b_{j,nm}/j_n(kr)$.

2.4. Extrapolation via Equivalent Source Method

The equivalent source method (ESM) is closely related to the plane wave decomposition method. Instead of plane waves, monopoles are chosen as basis functions which has the advantage that the decay of sound pressure with distance from the sources is taken into account with $H_{ij}^{\mathrm{ESM}} = \frac{1}{4\pi r_{ij}} e^{jkr_{ij}}$. $r_{ij} = \|\mathbf{r}_i - \mathbf{r}_j\|_2$ is the euclidean distance of an equivalent source to a measurement point. This way further physical knowledge is utilised and better reconstruction is expect. The locations of the equivalent sources are placed in a regular grid surrounding the sound sources. The sound sources are represented with multiple monopoles to extend their size according to the size of a membrane of a PA loud-speaker. Furthermore is a sound source always centered in between the grid of equivalent sources so that the results represent the worst case of the chosen configuration, see Figure 3. The ESM can be represented in matrix form like Equation 4 and the coefficients can be computed via inversion.

2.5. Inverse Problem

Ill posed inverse problems can be solved via minimisation utilising the ℓ_1-norm and ℓ_2-norm with

$$\mathbf{x}_{\ell_1} = \arg\min_{\mathbf{x}} \|\mathbf{x}\|_1, \quad \text{subject to } \|\mathbf{Hx} - \mathbf{p}\|_2 \leq \epsilon \tag{12}$$

and

$$\mathbf{x}_{\ell_2} = \arg\min_{\mathbf{x}} \|\mathbf{Hx} - \mathbf{p}\|_2 + \lambda\|\mathbf{x}\|_2. \tag{13}$$

In case of a sparse distribution of noise sources it might be beneficial to pose an ℓ_1-norm minimisation problem while in some cases the ℓ_2-norm could lead to better results, as will be shown.

ℓ_1-norm minimisation is also known as compressive sensing [9, 10] and ℓ_2-norm minimisation can be expressed as pseudo inverse. The constant ϵ in Equation 12 is an inequality constraint. A good choice for this constant has been experimentally investigated for the specific cases presented here and is $\epsilon = 20\sqrt{\mathbf{n}^T\mathbf{n}/M}$ for all three extrapolation methods. The constant λ in Equation 13 is the Tikhonov

regularisation factor which was different for each extrapolation method. The constant $\lambda = 1\sqrt{\mathbf{n}^T\mathbf{n}/M}$ has been chosen, which is an average that works well for all methods presented here. The ℓ_1-norm minimisation has been solved with the CVX library in Matlab. Equation 13 is a Least Mean Square approach which has been computed with the closed form regularised pseudo inverse

$$\mathbf{x}_{\ell_2} = (\mathbf{H}^*\mathbf{H} + \lambda\mathbf{I})^{-1}\mathbf{H}^*\mathbf{p}, \tag{14}$$

where * indicates the complex conjugate transposed.

3. RESULTS

In the following the accuracy of the reconstructing methods ESM, PWD and SHD is presented as sound-field plots and as the point-wise normalised mean square error (NMSE) in the xy-plane in which the spherical array is placed. The NMSE

$$\epsilon_{NMSE} = 10\log_{10}\left(\frac{|p_m - p_r|^2}{|p_m|^2}\right) \tag{15}$$

is related to the amount of noise reduction in the case of active noise control. p_m is the measured sound-field and p_r the reconstructed. If perfect reconstruction is possible with $\epsilon_{\mathrm{NMS}} = -\infty$, the maximum reduction of noise that is possible with active control is achievable. E.g. infinite reduction in a single channel active control setup without noise. Contour lines are added that indicate the region of stability in which adaptive control is stable when all other conditions are ideal, for example with $\tilde{\mathbf{G}}_{pu} = \mathbf{G}_{pu}$. In order to save space only the maximum phase error of all frequencies is shown, so the contour indicates only that there is a stability issue for at least one frequency.

$$\left|\tan^{-1}\left(\mathrm{Re}(\frac{p_m}{p_r})/\,\mathrm{Im}(\frac{p_m}{p_r})\right)\right| = |\Delta\phi| < \frac{\pi}{2}. \tag{16}$$

The reconstruction accuracy is shown for two different scenarios which are related to a specific active noise control problem where the primary noise consists of sources far away (50m) and the control speakers are close to the quiet zone area (2m). This project has been presented in [11]. It is the sound-field of the primary noise sources that is to be reconstructed and the sound field of the secondary sources respectively. A simple scenario is shown first, where the sound source is a single source in space, which is represented by a collection of monopoles to slightly extend its shape. Ground reflections are neglected. Figure 3 shows the more complex setup, which will be presented next, with enlarged sound sources, ground reflections and grids of equivalent sources. The grid density increases slightly with distance to account for increasing uncertainty in estimating the exact source locations the further away the sources are. Measurement noise is added with 35 dB SNR, which is realistic when the sound to be reconstructed is coming from the loud-speakers of a concert venue. The order of the SHD is manually truncated at $N = 2$ resulting in $(N + 1)^2 = 9$ modes. The measurement with 64 microphones supports SHD up to order 7 but the noise level of 35 dB contaminates the modes above order 2. The manual truncation reduces the impact of noise and leads to better results when the ℓ_2-norm is used.

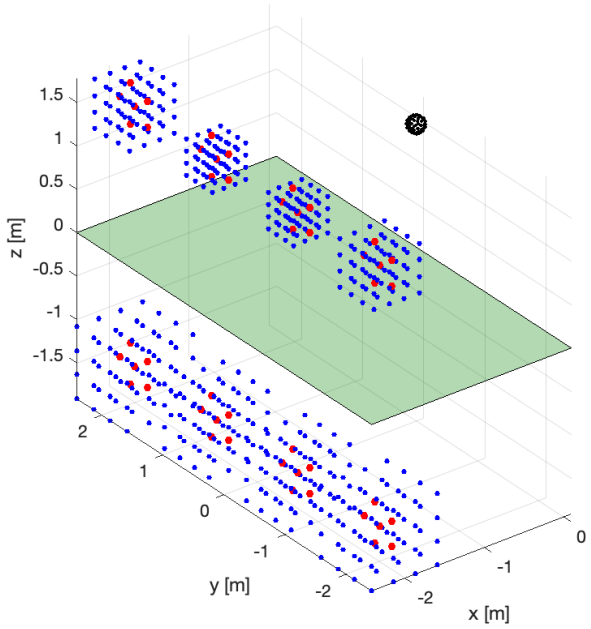

Figure 3: Example of a simulation configuration with 4 extended sound sources in 2m distance from the origin; spherical measurement array (black dots), monopoles representing the sound sources (red dots), sources of the ESM (blue dots), the ground with absorption coefficient 0.25 (green surface), the set of sources below the ground represent ground reflections

The following figures 4 and 5 show the sound-fields and the NMSE of reconstruction for a single extended source in 50m distance.

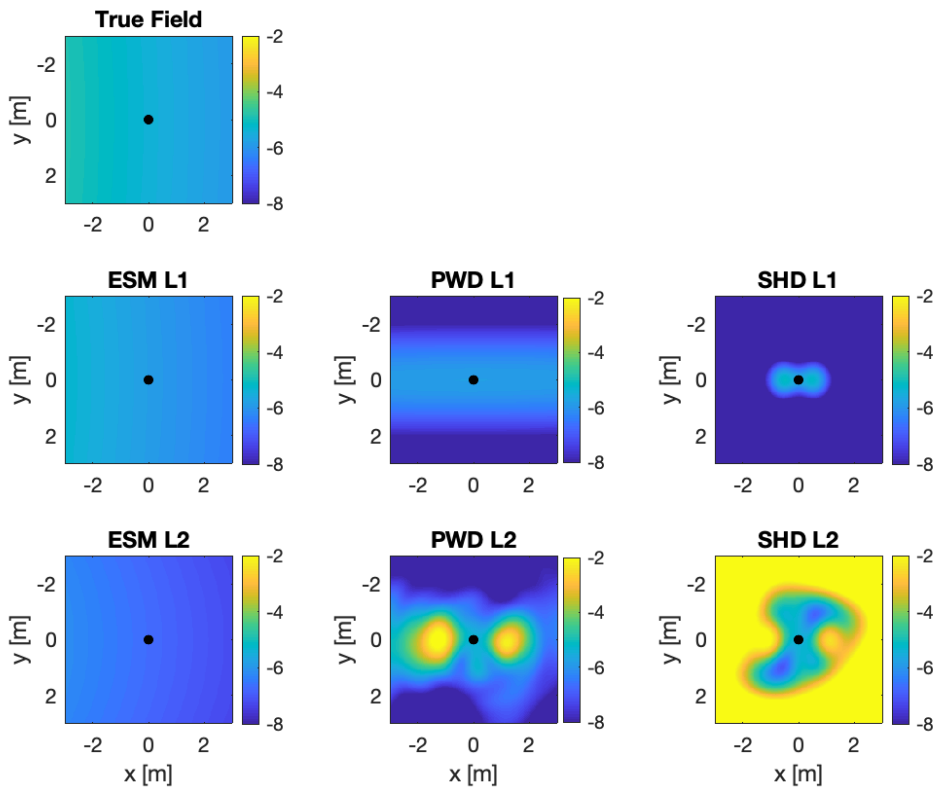

Figure 4: Normalised SPL of the true and reconstructed sound-fields of a single sound source in 50m distance, 35dB SNR, f = 10:10:200 (start:step:end)

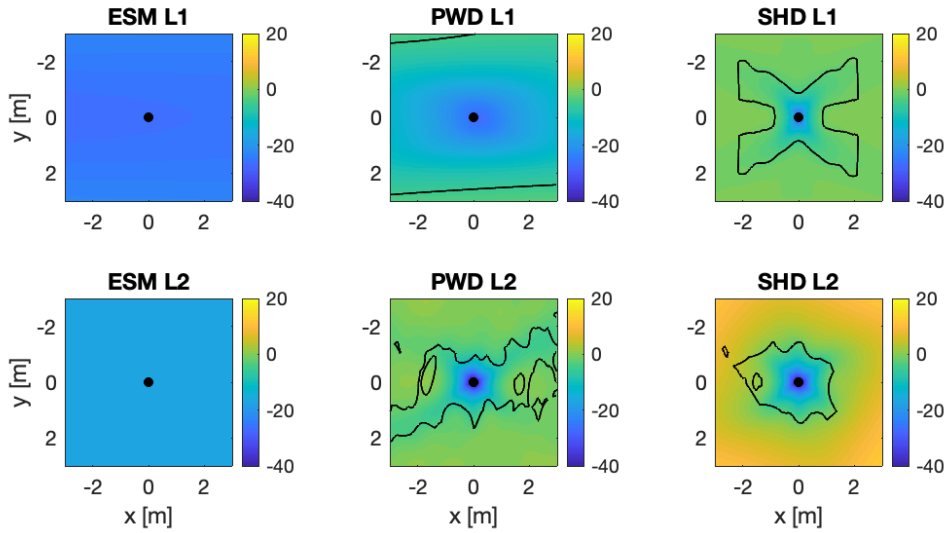

Figure 5: Reconstruction Error (NMSE) for a single sound source in 50m distance, 35dB SNR, contours indicate the region of stability $|\Delta\phi| < \pi/2$, f= 10:10:200 (start:step:end)

It can be seen that the ESM and PWD method with ℓ_1-norm and ESM with ℓ_2-norm provide stability with respect to active control throughout the whole presented area. PWD and SHD produce a very small region of stability in which active control would be possible at all with large reconstruction error. Figures 6 and 7 show the results for a source in 2m distance.

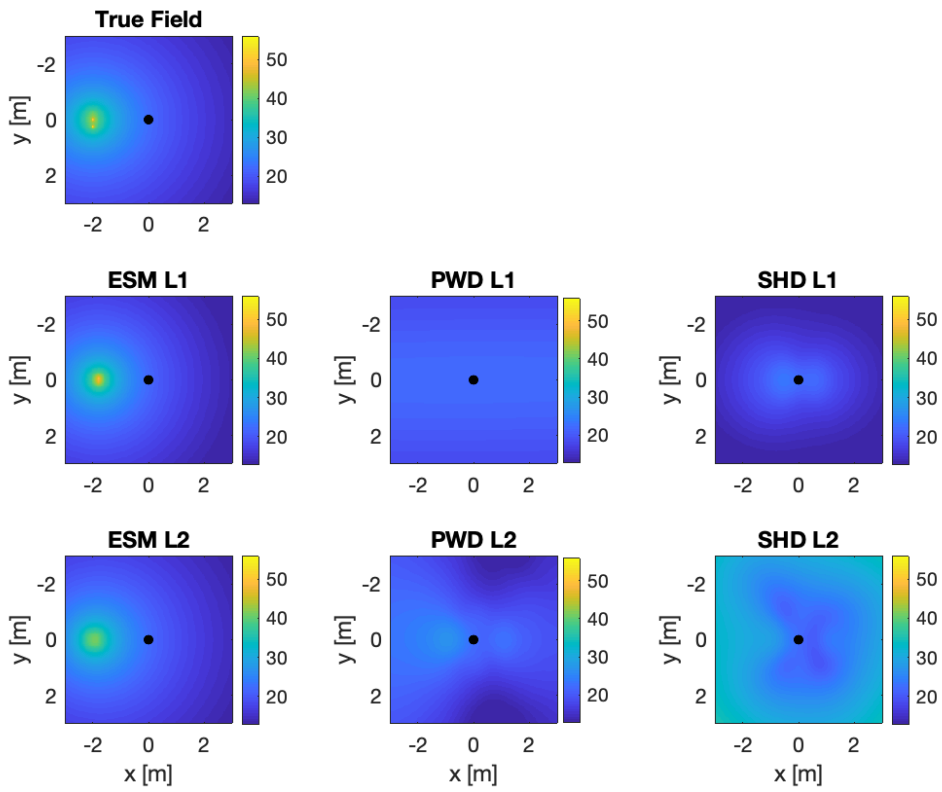

Figure 6: Normalised SPL of the true and reconstructed sound-fields of a single sound source in 2m distance, 35dB SNR, f = 10:10:200 (start:step:end)

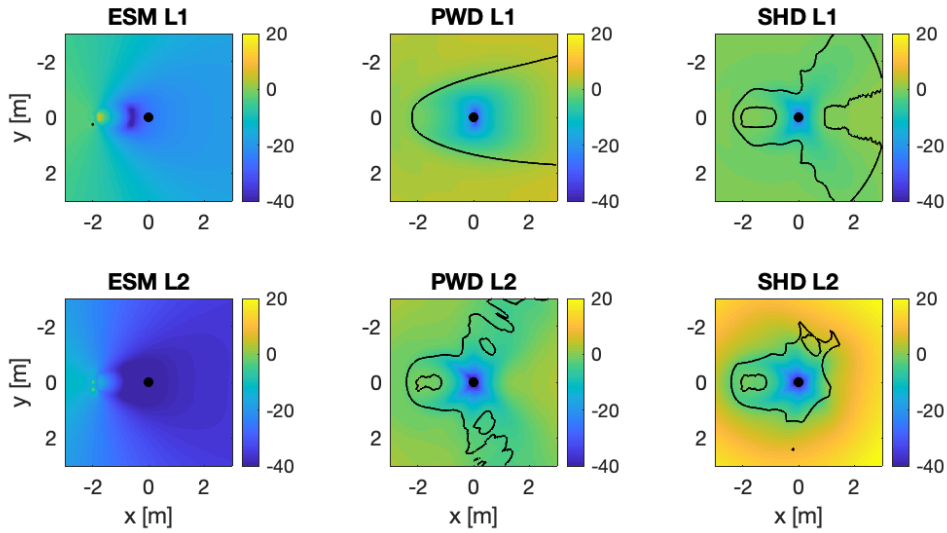

Figure 7: Reconstruction Error (NMSE) for a single sound source in 2m distance, 35dB SNR, contours indicate the region of stability $|\Delta\phi| < \pi/2$, f= 10:10:200 (start:step:end)

Here shows the ESM method with ℓ_2-norm much better performance and the PWD with ℓ_1-norm performs worse on the other hand. It is harder to synthesise the curved sound field of a close sound source with a limited number of plane waves than a nearly plane sound field from a source far away. The ESM with ℓ_2-norm performs better for a close source because in the particular case presented here it is beneficial to fit more equivalent sources to the large sound source (modeled by 6

monopoles). The ℓ_1-norm minimises the number of equivalent sources resulting in only a few active coefficients that represent the sound source worse. This specific result depends on the chosen grid of equivalent sources. When the grid covers a bigger volume with equivalent sources further away is the performance of the ℓ_2-norm decreased and similar to ℓ_1. Such a case is represented in Figure 8 where a wide and dense grid of equivalent sources has been used. When measurement noise is very low then ℓ_1-norm and ℓ_2-norm perform very well and equally well. Plots with noiseless results are omitted here.

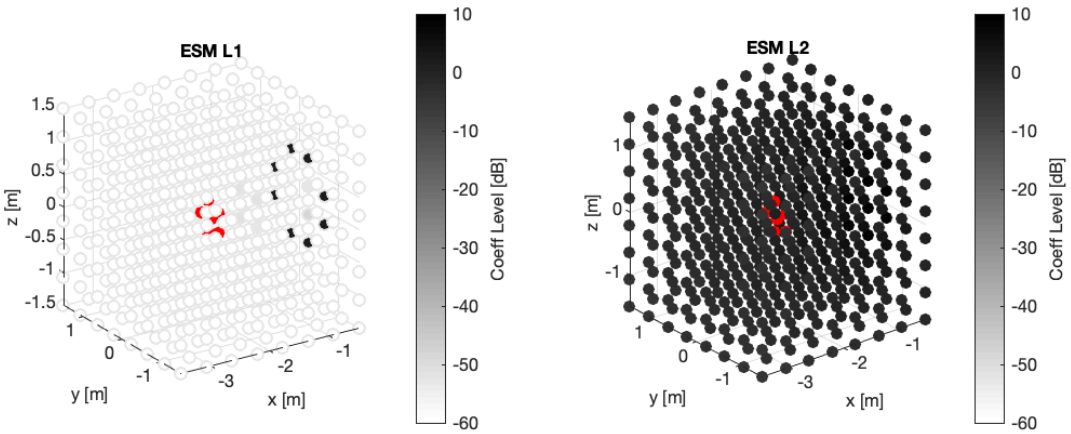

Figure 8: Coefficients of the ESM basis functions (equivalent sources) for the ℓ_1-norm (left) and ℓ_2-norm (right), points in gray scale are the coefficients, red points represent the sound source.

Figures 9 and 10 present more complex scenarios where 4 sound sources are placed in 50m and 2m distance respectively. Moreover are ground reflections included, see Figure 3 for the configuration. The sound-field plots showing the true and reconstructed sound fields are omitted because of space limitations.

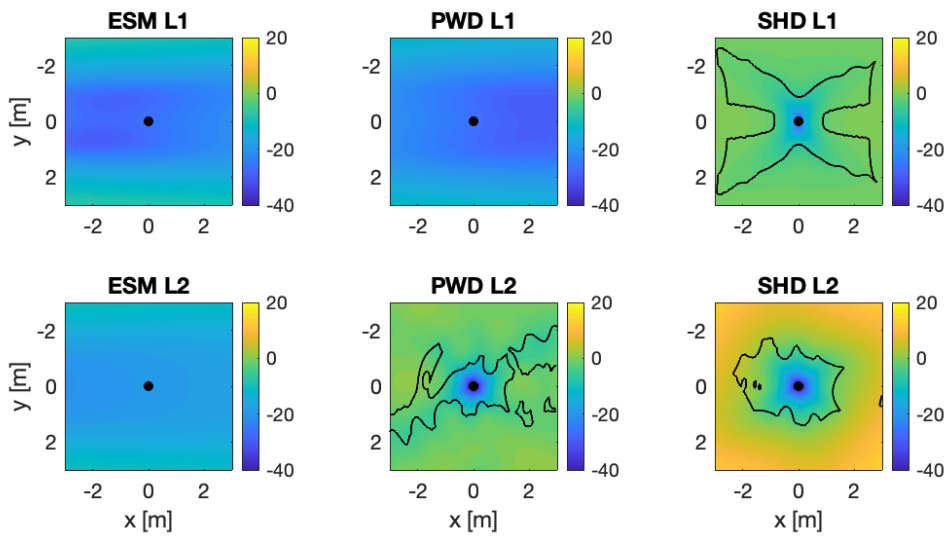

Figure 9: Reconstruction Error (NMSE) for 4 sound sources in 50m distance, 35dB SNR, contours indicate the region of stability $|\Delta\phi| < \pi/2$, f=10:10:200 (start:step:end)

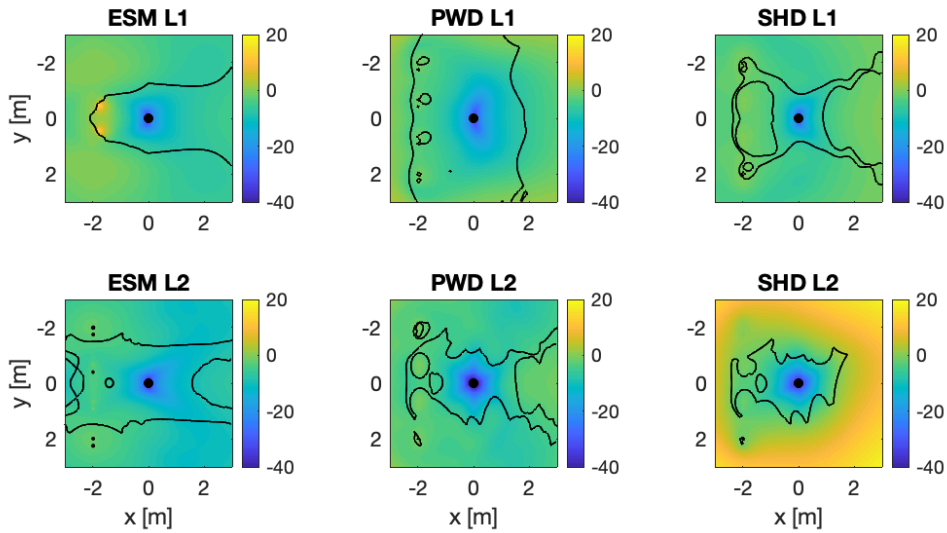

Figure 10: Reconstruction Error (NMSE) for 4 sound sources in 2m distance, 35dB SNR, contours indicate the region of stability $|\Delta\phi| < \pi/2$, f=10:10:200 (start:step:end)

The PWD with ℓ_1-norm handles the distant array of sources slightly better than a single source. Multiple sources in a distant linear array produce a more plane sound field that is easier to fit for the PWD method. The ground reflections just shape another plane wave with lower level which can be fitted well, too. The ESM and PWD with ℓ_1-norm show good reconstruction in the overall presented region while SHD and PWD with ℓ_2-norm produce large errors even close to the measurement sphere. Close sources with ground reflections are hard to handle by all the methods. The ESM based reconstructions seem to produce a longer corridor of stable reconstruction on the x axis, in line of sight with the sound source array, but with a NMSE of only $\approx -10dB$. Note that the region of stable reconstruction with respect to active control always surrounds the measurement array. The symmetry of the contour lines is corrupted by the noise.

4. DISCUSSION

The results have shown that reconstruction of sources far away is possible in a bigger area with a NMSE $< 20dB$. The same is true for multiple sources in a linear array and with ground reflections. It could further be validated that reflections on close by objects could be fitted as well, when the main source is far away. These simulations were omitted because of space limitations. Note that the results presented are bound to a specific scenario of active noise control on which the choice for the presented source configuration is based. Randomly distributed sources have not been investigated e.g. and might produce worse results. On the other hand might a different shape of the sound source arrays produce better results. A curved array in 2m distance has shown some improvement with the ESM e.g. Also these results are omitted.

Moreover is the sampling of the sound field a critical element. While a spherical measurement array might be best suited for the SHD method so can a different sampling scheme support one of the others. Compressive sensing e.g. relies on incoherent measurements, so a randomised sampling could improve the reconstruction accuracy.

The grid size of the ESM affects the accuracy of reconstruction. A wide grid of sources can account for reflections and unexpected noise sources but the performance using the ℓ_2-norm will suffer when noise is present. At the same time can the ℓ_1-norm lead to worse results for close sources, when the sources are large. ℓ_1 minimises the number of active coefficients while many would be needed to synthesize large sound sources.

The SHD has generally shown minor performance. When very low measurement noise is present,

the SHD can show better reconstruction and even outperform the PWD. Simulations with low noise are omitted because noise is generally present in realistic scenarios of active noise control.

5. CONCLUSIONS

Good reconstruction is achievable for sources far away with the ESM and PWD method. Therefore are these valid candidates for the integration into the MBRMT. On the other hand are close sound sources hard to fit by all methods when ground reflections and noise are present. Therefore are the investigated methods finally critical for the application in the MBRMT since the prediction of the contribution of the close secondary sources in the virtual error sensing location is an important element of the MBRMT. The sampling scheme of the measurement array and the secondary source configuration can still be optimised and might lead to better reconstruction, also for close sources.

Apart from that is the utilisation of the ℓ_1-norm recommended when noise is present and the sources are far away. The ℓ_2-norm seems to work better for close sources but suffers like the ℓ_1-norm when noise and ground are present. Note that the computation of the ℓ_1-norm minimisation is computationally much more expensive than the ℓ_2-norm which can be applied via pseudo-inverse. The computational effort is critical for ANC applications.

6. REFERENCES

[1] D. Moreau, B. Cazzolato, A. Zander, and C. Petersen, "A review of virtual sensing algorithms for active noise control," *Algorithms*, vol. 1, no. 2, pp. 69–99, 2008.

[2] S. Elliot, *Signal Processing for Active Control*. Academic Press, 2001.

[3] A. Roure and A. Albarrazin, "The Remote Microphone Technique for Active Noise Control," *Proceedings of Active 99*, 1999.

[4] C. H. Hansen, S. Snyder, X. Qiu, L. Brooks, and D. Moreau, *Active control of noise and vibration*, vol. I+II. Taylor & Francis, 2nd editio ed., 2012.

[5] F. M. Heuchel, D. C. Nozal, F. T. Agerkvist, and J. Brunskog, "Sound field control for reduction of noise from outdoor concerts," *145th Audio Engineering Society International Convention, AES 2018*, 2018.

[6] A. Moiola, R. Hiptmair, and I. Perugia, "Plane wave approximation of homogeneous Helmholtz solutions," *Zeitschrift fur Angewandte Mathematik und Physik*, vol. 62, no. 5, pp. 809–837, 2011.

[7] E. G. Williams, *Fourier Acoustics*. Academic Press, 1999.

[8] B. Rafaely, *Springer Topics in Signal Processing Fundamentals of Spherical Array Processing*. Springer Nature Switzerland AG 2019, 2nd ed., 2015.

[9] E. Fernandez-Grande, "Sound field reconstruction using a spherical microphone array," *The Journal of the Acoustical Society of America*, vol. 139, no. 3, pp. 1168–1178, 2016.

[10] S. A. Verburg and E. Fernandez-Grande, "Reconstruction of the sound field in a room using compressive sensing," *The Journal of the Acoustical Society of America*, vol. 143, no. 6, pp. 3770–3779, 2018.

[11] D. Plewe, F. T. Agerkvist, and J. Brunskog, "A quiet zone system, optimized for large outdoor events, based on multichannel FxLMS ANC," *145th Audio Engineering Society International Convention, AES 2018*, 2018.